

The Nuclear Equation of State at high densities

Christian Fuchs

*Institut für Theoretische Physik,
Universität Tübingen,*

D-72076 Tübingen, Germany

E-mail: christian.fuchs@uni-tuebingen.de

Ab initio calculations for the nuclear many-body problem make predictions for the density and isospin dependence of the nuclear equation-of-state (EOS) far away from the saturation point of nuclear matter. I compare predictions from microscopic and phenomenological approaches. Constraints on the EOS derived from heavy ion reactions, in particular from subthreshold kaon production, as well as constraints from neutron stars are discussed.

1. Introduction

Heavy ion reactions provide the only possibility to reach nuclear matter densities beyond saturation density $\rho_0 \simeq 0.16 \text{ fm}^{-3}$. Transport calculations indicate that in the low and intermediate energy range $E_{\text{lab}} \sim 0.1 \div 1$ AGeV nuclear densities between $2 \div 3\rho_0$ are accessible while the highest baryon densities ($\sim 8\rho_0$) will probably be reached in the energy range of the future GSI facility FAIR between $20 \div 30$ AGeV. At even higher incident energies transparency sets in and the matter becomes less baryon rich due to the dominance of meson production. The isospin dependence of the nuclear forces which is at present only little constrained by data will be explored by the forthcoming radioactive beam facilities at FAIR/GSI ¹, SPIRAL2/GANIL and RIA ². Since the knowledge of the nuclear equation-of-state (EOS) at supra-normal densities and extreme isospin is essential for our understanding of the nuclear forces as well as for astrophysical purposes, the determination of the EOS was already one of the primary goals when first relativistic heavy ion beams started to operate in the beginning of the 80ties. In the following I briefly discuss the knowledge about the nuclear EOS at *moderate densities and temperatures*. For more details see e.g. Ref. ³.

Models which make predictions on the nuclear EOS can roughly be di-

vided into three classes: *phenomenological density functionals* such as Gogny or Skyrme forces ^{4, 5, 6} and relativistic mean field (RMF) models ⁷, *effective field theory* (EFT) and *ab initio approaches*. In EFT a systematic expansion of the EOS in powers of density, respectively the Fermi momentum k_F is performed. EFT can be based on density functional theory ^{8, 9} or e.g. on chiral perturbation theory ^{10, 11, 12}. Ab initio approaches are used on high precision free space nucleon-nucleon interactions and the nuclear many-body problem is treated microscopically. Predictions for the nuclear EOS are essentially parameter free. Examples are variational calculations ¹³, Brueckner-Hartree-Fock (BHF) ^{14, 15} or relativistic Dirac-Brueckner-Hartree-Fock (DBHF) ^{16, 17, 18} and Greens functions Monte-Carlo approaches ^{19, 20}. In the following I will mainly concentrate on the DBHF approach.

2. The EOS from ab initio calculations

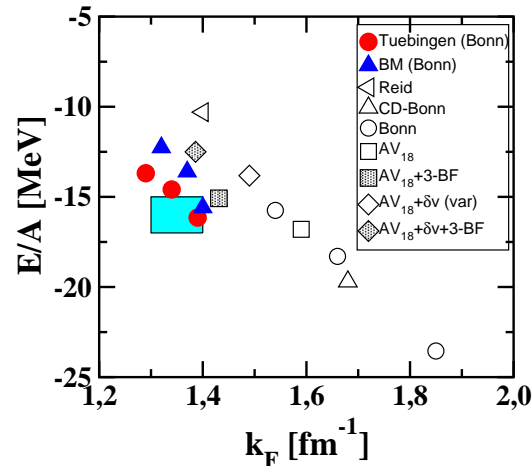


Fig. 1. Nuclear matter saturation points from relativistic (full symbols) and non-relativistic (open symbols) Brueckner-Hartree-Fock calculations based on different nucleon-nucleon forces. The diamonds show results from variational calculations. Shaded symbols denote calculations which include 3-body forces. The shaded area is the empirical region of saturation. Figure is taken from Ref. ²¹.

In *ab initio* calculations based on many-body techniques one derives the energy functional from first principles, i.e. treating short-range and many-body correlations explicitly. A typical example for a successful many-body

approach is Brueckner theory²². In the relativistic Brueckner approach the nucleon inside the medium is dressed by the self-energy Σ . The in-medium T-matrix which is obtained from the relativistic Bethe-Salpeter (BS) equation plays the role of an effective two-body interaction which contains all short-range and many-body correlations of the ladder approximation. Solving the BS-equation the Pauli principle is respected and intermediate scattering states are projected out of the Fermi sea. The summation of the T-matrix over the occupied states inside the Fermi sea yields finally the self-energy in Hartree-Fock approximation. This coupled set of equations states a self-consistency problem which has to be solved by iteration.

In contrast to relativistic DBHF calculations which came up in the late 80ties non-relativistic BHF theory has already almost half a century's history. The first numerical calculations for nuclear matter were carried out by Brueckner and Gammel in 1958²². Despite strong efforts invested in the development of improved solution techniques for the Bethe-Goldstone (BG) equation, the non-relativistic counterpart of the BS equation, it turned out that, although such calculations were able to describe the nuclear saturation mechanism qualitatively, they failed quantitatively. Systematic studies for a large number of NN interactions were always allocated on a so-called *Coester-line* in the $E/A - \rho$ plane which does not meet the empirical region of saturation. In particular modern one-boson-exchange (OBE) potentials lead to strong over-binding and too large saturation densities where relativistic calculations do a much better job.

Fig. 1 compares the saturation points of nuclear matter obtained by relativistic Dirac-Brueckner-Hartree-Fock (DBHF) calculations using the Bonn potentials²³ as bare NN interactions to non-relativistic Brueckner-Hartree-Fock calculations for various NN interactions. The DBHF results are taken from Ref.²⁴ (BM) and more recent calculations based on improved techniques are from Ref.¹⁷ (Tübingen). Several reasons have been discussed in the literature in order to explain the success of the relativistic treatment (see e.g. discussion in Ref.²⁵). Three-body forces (3-BFs) have extensively been studied within non-relativistic BHF¹⁴ and variational calculations¹³. Both approaches shown in Fig. 2 are based on the latest AV₁₈ version of the Argonne potential. The variational results shown contain boost corrections (δv) which account for relativistic kinematics and lead to additional repulsion¹³.

The contributions from 3-BFs are in total repulsive which makes the EOS harder and non-relativistic calculations come close to their relativistic counterparts. The same effect is observed in variational calculations¹³

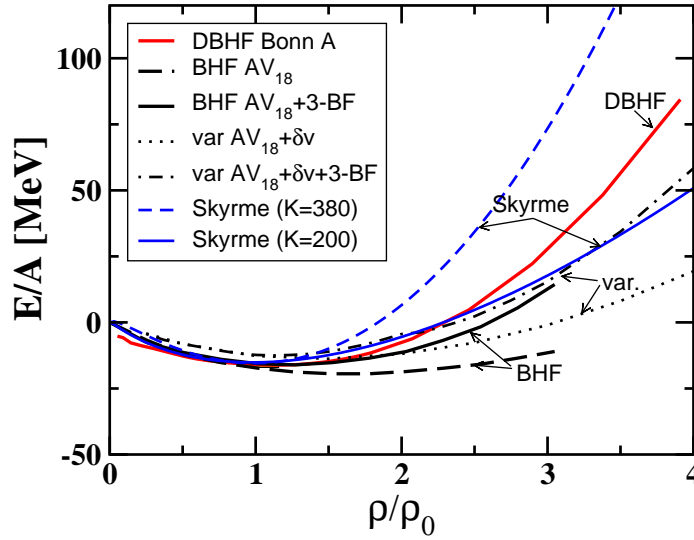


Fig. 2. Predictions for the EOS of symmetric nuclear matter from microscopic ab initio calculations, i.e. relativistic DBHF¹⁷, non-relativistic BHF¹⁴ and variational¹³ calculations. For comparison also soft and hard Skyrme forces are shown. Figure is taken from Ref.²¹.

shown in Fig. 2. It is often argued that in non-relativistic treatments 3-BFs play in some sense an equivalent role as the dressing of the two-body interaction by in-medium spinors in Dirac phenomenology. Both mechanisms lead indeed to an effective density dependent two-body interaction V which is, however, of different origin. One class of 3-BFs involves virtual excitations of nucleon-antinucleon pairs. Such Z-graphs are in net repulsive and can be considered as a renormalization of the meson vertices and propagators. A second class of 3-BFs is related to the inclusion of explicit resonance degrees of freedom. The most important resonance is the $\Delta(1232)$ isobar which provides at low and intermediate energies large part of the intermediate range attraction.

Fig. 2 compares the equations of state from the different approaches: DBHF from Ref.¹⁷ based the Bonn A interaction^{a 23}, BHF¹⁴ and variational calculations¹³. The latter ones are based on the Argonne AV₁₈ potential and include 3-body forces. All the approaches use modern high precision NN interactions and represent state of the art calculations. Two phe-

^aThe high density behavior of the EOS obtained with different interaction, e.g. Bonn B or C is very similar.¹⁷

nomenological Skyrme functionals which correspond to the limiting cases of a soft ($K=200$ MeV) and a hard ($K=380$ MeV) EOS are shown as well. In contrast to the Skyrme interaction where the high density behavior is fixed by the parameters which determine the compression modulus, in microscopic approaches the compression modulus is only loosely connected to the curvature at saturation density. DBHF Bonn A has e.g. a compressibility of $K=230$ MeV. Below $3\rho_0$ both are not too far from the soft Skyrme EOS. The same is true for BHF including 3-body forces.

When many-body calculations are performed, one has to keep in mind that elastic NN scattering data constrain the interaction only up to about 400 MeV, which corresponds to the pion threshold. NN potentials differ essentially in the treatment of the short-range part. A model independent representation of the NN interaction can be obtained in EFT approaches where the unresolved short distance physics is replaced by simple contact terms. In the framework of chiral EFT the NN interaction has been computed up to $N^3\text{LO}$ ^{26, 27}. An alternative approach which leads to similar results is based on renormalization group (RG) methods ²⁸. In the $V_{\text{low } k}$ approach a low-momentum potential is derived from a given realistic NN potential by integrating out the high-momentum modes using RG methods. When applied to the nuclear many-body problem low momentum interactions do not require a full resummation of the Brueckner ladder diagrams but can already be treated within second-order perturbation theory ²⁹. However, without repulsive three-body-forces isospin saturated nuclear matter was found to collapse. Including 3-BFs first promising results have been obtained with $V_{\text{low } k}$ ²⁹, however, nuclear saturation is not yet described quantitatively.

2.1. *EOS in symmetric and asymmetric nuclear matter*

Fig. 3 compares now the predictions for nuclear and neutron matter from microscopic many-body calculations – DBHF ¹⁸ and the 'best' variational calculation with 3-BFs and boost corrections ¹³ – to phenomenological approaches and to EFT. As typical examples for relativistic functionals we take NL3 ³⁰ as one of the best RMF fits to the nuclear chart and a phenomenological density dependent RMF functional DD-TW from Ref. ³¹. ChPT+corr. is based on chiral pion-nucleon dynamics ¹¹ including condensate fields and fine tuning to finite nuclei. As expected the phenomenological functionals agree well at and below saturation density where they are constrained by finite nuclei, but start to deviate substantially at supra-normal densities. In neutron matter the situation is even worse since the

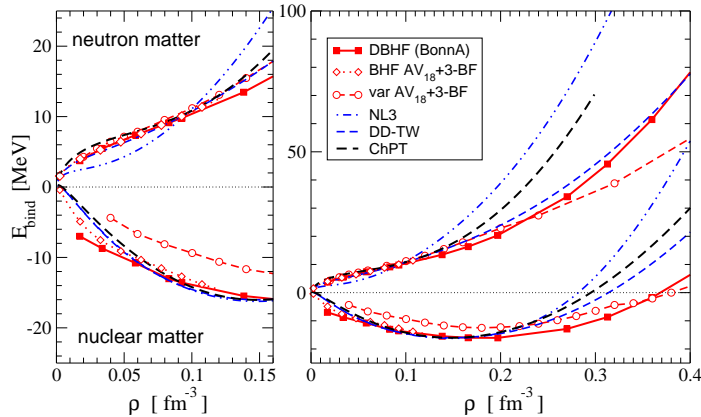


Fig. 3. EOS in nuclear matter and neutron matter. BHF/DBHF and variational calculations are compared to phenomenological density functionals NL3 and DD-TW and ChPT+corr.. The left panel zooms the low density range. The Figure is taken from Ref. 3.

isospin dependence of the phenomenological functionals is less constrained. The predictive power of such density functionals at supra-normal densities is restricted. *Ab initio* calculations predict throughout a soft EOS in the density range relevant for heavy ion reactions at intermediate and low energies, i.e. up to about three times ρ_0 . There seems to be no way to obtain an EOS as stiff as the hard Skyrme force shown in Fig. 2 or NL3. Since the *nn* scattering length is large, neutron matter at subnuclear densities is less model dependent. The microscopic calculations (BHF/DBHF, variational) agree well and results are consistent with 'exact' Quantum-Monte-Carlo calculations²⁰.

In isospin asymmetric matter the binding energy is a functional of the proton and neutron densities, characterized by the asymmetry parameter $\beta = Y_n - Y_p$ which is the difference of the neutron and proton fraction $Y_i = \rho_i/\rho$, $i = n, p$. The isospin dependence of the energy functional can be expanded in terms of β which leads to a parabolic dependence on the asymmetry parameter

$$E(\rho, \beta) = E(\rho) + E_{\text{sym}}(\rho)\beta^2 + \mathcal{O}(\beta^4) + \dots$$

$$E_{\text{sym}}(\rho) = \frac{1}{2} \frac{\partial^2 E(\rho, \beta)}{\partial \beta^2} \Big|_{\beta=0} = a_4 + \frac{p_0}{\rho_0^2}(\rho - \rho_0) + \dots \quad (1)$$

Fig. 4 compares the symmetry energy predicted from the DBHF and variational calculations to that of the empirical density functionals already shown in Fig. 3 In addition the relativistic DD- $\rho\delta$ RMF functional³² is in-

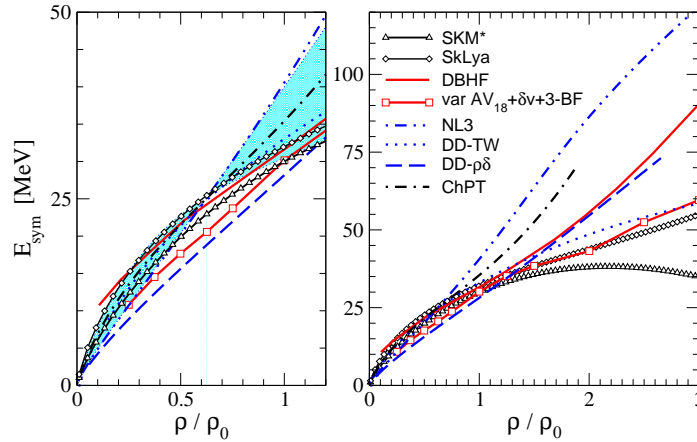


Fig. 4. Symmetry energy as a function of density as predicted by different models. The left panel shows the low density region while the right panel displays the high density range. The Figure is taken from Ref. ³.

cluded. Two Skyrme functionals, SkM* and the more recent Skyrme-Lyon force SkLya represent non-relativistic models. The left panel zooms the low density region while the right panel shows the high density behavior of E_{sym} . Remarkable is that most empirical models coincide around $\rho \simeq 0.6\rho_0$ where $E_{\text{sym}} \simeq 24$ MeV. This demonstrates that constraints from finite nuclei are active for an average density slightly above half saturation density. However, the extrapolations to supra-normal densities diverge dramatically. This is crucial since the high density behavior of E_{sym} is essential for the structure and the stability of neutron stars (see also the discussion in Sec. V.5). The microscopic models show a density dependence which can still be considered as *asy-stiff*. DBHF ¹⁸ is thereby stiffer than the variational results of Ref. ¹³. The density dependence is generally more complex than in RMF theory, in particular at high densities where E_{sym} shows a non-linear and more pronounced increase. Fig. 4 clearly demonstrates the necessity to constrain the symmetry energy at supra-normal densities with the help of heavy ion reactions.

The hatched area in Fig. 4 displays the range of E_{sym} which has been obtained by constructing a density dependent RMF functional varying thereby the linear asymmetry parameter a_4 from 30 to 38 MeV ³³. In Ref. ³³ it was concluded that charge radii, in particular the skin thickness $r_n - r_p$ in heavy nuclei constrains the allowed range of a_4 to $32 \div 36$ MeV for relativistic functionals.

2.1.1. *Effective nucleon masses*

The introduction of an effective mass is a common concept to characterize the quasi-particle properties of a particle inside a strongly interacting medium. In nuclear physics exist different definitions of the effective nucleon mass which are often compared and sometimes even mixed up: the non-relativistic effective mass m_{NR}^* and the relativistic Dirac mass m_D^* . These two definitions are based on different physical concepts. The non-relativistic mass parameterizes the momentum dependence of the single-particle potential. The relativistic Dirac mass is defined through the scalar part of the nucleon self-energy in the Dirac field equation which is absorbed into the effective mass $m_D^* = M + \Sigma_S(k, k_F)$. The Dirac mass is a smooth function of the momentum. In contrast, the nonrelativistic effective mass - as a model independent result - shows a narrow enhancement near the Fermi surface due to an enhanced level density³⁴. For a recent review on this subject and experimental constraints on m_{NR}^* see Ref.³⁵.

While the Dirac mass is a genuine relativistic quantity the effective mass m_{NR}^* is determined by the single-particle energy

$$m_{NR}^* = k[dE/dk]^{-1} = \left[\frac{1}{M} + \frac{1}{k} \frac{d}{dk} U \right]^{-1}. \quad (2)$$

m_{NR}^* is a measure of the non-locality of the single-particle potential U (real

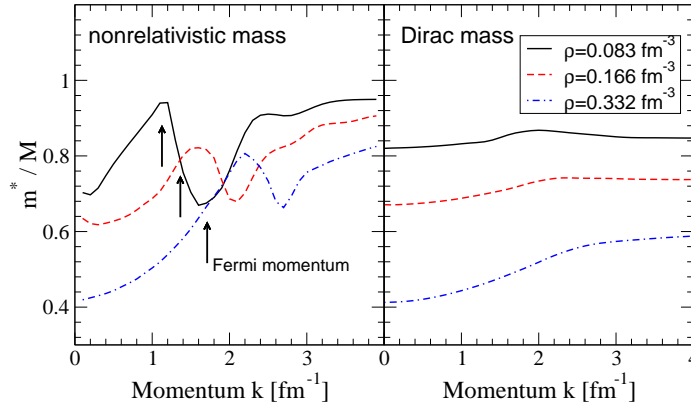


Fig. 5. The effective mass in isospin symmetric nuclear matter as a function of the momentum k at different densities determined from relativistic Brueckner calculations. Figure is taken from Ref.³⁶.

part) which can be due to non-localities in space, resulting in a momen-

tum dependence, or in time, resulting in an energy dependence. In order to clearly separate both effects, one has to distinguish further between the so-called k-mass and the E-mass³⁷. The spatial non-localities of U are mainly generated by exchange Fock terms and the resulting k-mass is a smooth function of the momentum. Non-localities in time are generated by Brueckner ladder correlations due to the scattering to intermediate states which are off-shell. These are mainly short-range correlations which generate a strong momentum dependence with a characteristic enhancement of the E-mass slightly above the Fermi surface^{34, 37, 38}. The effective mass defined by Eq. (2) contains both, non-localities in space and time and is given by the product of k-mass and E-mass³⁷. In Fig. 5 the nonrelativistic effective mass and the Dirac mass, both determined from DBHF calculations³⁶, are shown as a function of momentum k at different Fermi momenta of $k_F = 1.07, 1.35, 1.7 \text{ fm}^{-1}$. m_{NR}^* shows the typical peak structure as a function of momentum around k_F which is also seen in BHF calculations³⁸. The peak reflects the increase of the level density due to the vanishing imaginary part of the optical potential at k_F which is also seen, e.g., in shell model calculations^{34, 37}. One has, however, to account for correlations beyond mean field or Hartree-Fock in order to reproduce this behavior. Fig. 6 compares the density dependence of the two effective

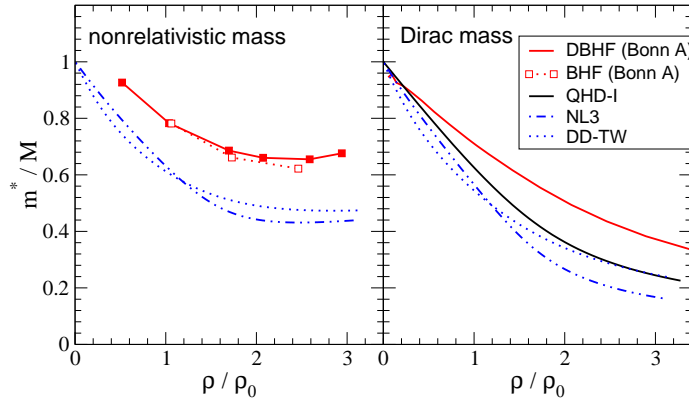


Fig. 6. Nonrelativistic and Dirac effective mass in isospin symmetric nuclear matter as a function of the density for various models.

masses determined at k_F . Both masses decrease with increasing density, the Dirac mass continuously, while m_{NR}^* starts to rise again at higher densities. Phenomenological density functionals (QHD-I, NL3, DD-TW) yield sys-

tematically smaller values of m_{NR}^* than the microscopic approaches. This reflects the lack of nonlocal contributions from short-range and many-body correlations in the mean field approaches.

2.1.2. Proton-neutron mass splitting

A heavily discussed topic is in the moment the proton-neutron mass splitting in isospin asymmetric nuclear matter. This question is of importance for the forthcoming new generation of radioactive beam facilities which are devoted to the investigation of the isospin dependence of the nuclear forces at its extremes. However, presently the predictions for the isospin dependences differ substantially. BHF calculations^{14, 38} predict a proton-neutron mass splitting of $m_{NR,n}^* > m_{NR,p}^*$. This stands in contrast to relativistic mean-field (RMF) theory. When only a vector isovector ρ -meson is included Dirac phenomenology predicts equal masses $m_{D,n}^* = m_{D,p}^*$ while the inclusion of the scalar isovector δ -meson, i.e. $\rho + \delta$, leads to $m_{D,n}^* < m_{D,p}^*$ ³². When the effective mass is derived from RMF theory, it shows the same behavior as the corresponding Dirac mass, namely $m_{NR,n}^* < m_{NR,p}^*$ ³². Conventional Skyrme forces, e.g. SkM*, lead to $m_{NR,n}^* < m_{NR,p}^*$ ³⁹ while the more recent Skyrme-Lyon interactions (SkLya) predict the same mass splitting as RMF theory. The predictions from relativistic DBHF calculations are in the literature still controversial. They depend strongly on approximation schemes and techniques used to determine the Lorentz and the isovector structure of the nucleon self-energy. Projection techniques are involved but more accurate and yield the same mass splitting as found in RMF theory when the δ -meson is included, i.e. $m_{D,n}^* < m_{D,p}^*$ ^{18, 40}. Recently also the non-relativistic effective mass has been determined with the DBHF approach and here a reversed proton-neutron mass splitting was found, i.e. $m_{NR,n}^* > m_{NR,p}^*$ ³⁶. Thus DBHF is in agreement with the results from nonrelativistic BHF calculations.

2.1.3. Optical potentials

The second important quantity related to the momentum dependence of the mean field is the optical nucleon-nucleus potential. At subnormal densities the optical potential U_{opt} is constraint by proton-nucleus scattering data⁴¹ and at supra-normal densities constraints can be derived from heavy ion reactions, see Refs.^{42, 43, 44}. In a relativistic framework the optical

Schroedinger-equivalent nucleon potential (real part) is defined as

$$U_{\text{opt}} = -\Sigma_S + \frac{E}{M}\Sigma_V + \frac{\Sigma_S^2 - \Sigma_V^2}{2M}. \quad (3)$$

One should thereby note that in the literature sometimes also an optical potential, given by the difference of the single-particle energies in medium and free space $U = E - \sqrt{M^2 + \mathbf{k}^2}$ is used⁴² which should be not mixed up with (3). In a relativistic framework momentum independent fields $\Sigma_{S,V}$ (as e.g. in RMF theory) lead always to a linear energy dependence of U_{opt} . As seen from Fig. 7 DBHF reproduces the empirical optical potential⁴¹ extracted from proton-nucleus scattering for nuclear matter at ρ_0 reasonably well up to a laboratory energy of about 0.6-0.8 GeV. However, the saturating behavior at large momenta cannot be reproduced by this calculations because of missing inelasticities, i.e. the excitation of isobar resonances above the pion threshold. When such continuum excitations are accounted for optical model calculations are able to describe nucleon-nucleus scattering data also at higher energies⁴⁵. In heavy ion reactions at incident energies above 1 AGeV such a saturating behavior is required in order to reproduce transverse flow observables⁴⁴. One has then to rely on phenomenological approaches where the strength of the vector potential is artificially suppressed, e.g. by the introduction of additional form factors⁴⁴ or by energy dependent terms in the QHD Lagrangian⁴⁶ (D³C model in Fig.7).

The isospin dependence, expressed by the isovector optical potential $U_{\text{iso}} = (U_{\text{opt,n}} - U_{\text{opt,p}})/(2\beta)$ is much less constrained by data. The knowledge of this quantity is, however, of high importance for the forthcoming radioactive beam experiments. The right panel of Fig. 7 compares the predictions from DBHF¹⁸ and BHF⁴⁷ to the phenomenological Gogny and Skyrme (SkM* and SkLya) forces and a relativistic $T - \rho$ approximation⁴⁹ based on empirical NN scattering amplitudes⁵⁰. At large momenta DBHF agrees with the tree-level results of Ref.⁴⁹. While the dependence of U_{iso} on the asymmetry parameter β is found to be rather weak^{18, 47}, the predicted energy and density dependences are quite different, in particular between the microscopic and the phenomenological approaches. The energy dependence of U_{iso} is very little constrained by data. The old analysis of optical potentials of scattering on charge asymmetric targets by Lane⁵¹ is consistent with a decreasing potential as predicted by DBHF/BHF, while more recent analyses based on Dirac phenomenology⁵² come to the opposite conclusions. RMF models show a linearly increasing energy dependence of U_{iso} (i.e. quadratic in k) like SkLya, however generally with a smaller slope (see discussion in Ref.³²). To clarify this question certainly more

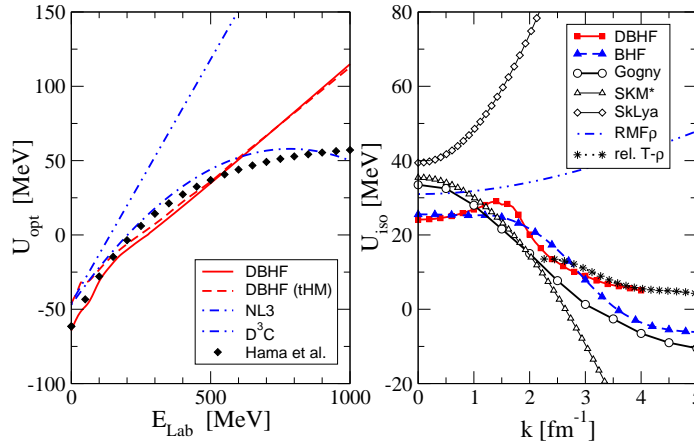


Fig. 7. Nucleon optical potential in nuclear matter at ρ_0 . On the left side DBHF calculations for symmetric nuclear matter from ¹⁶ and ¹⁷ are compared to the phenomenological models NL3 and D³C ⁴⁶ and to the p-A scattering analysis of ⁴¹. The right panel compares the iso-vector optical potential from DBHF ¹⁸ and BHF ⁴⁷ to phenomenological RMF ⁴⁸, Gogny and Skyrme forces and to a relativistic $T - \rho$ approximation ⁴⁹.

experimental efforts are necessary.

2.2. Probing the EOS by kaon production in heavy ion reactions

With the start of the first relativistic heavy ion programs the hope was that particle production would provide a direct experimental access to the nuclear EOS ⁵³. It was expected that the compressional energy should be released into the creation of new particles, primarily pions, when the matter expands ⁵³. However, pions have large absorption cross sections and they turned out not to be suitable messengers of the compression phase. They undergo several absorption cycles through nucleon resonances and freeze out at final stages of the reaction and at low densities. Hence pions lose most of their knowledge on the compression phase and are not very sensitive probes for stiffness of the EOS.

After pions turned out to fail as suitable messengers, K^+ mesons were suggested as promising tools to probe the nuclear EOS ⁵⁴. At subthreshold energies K^+ mesons are produced in the high density phase and due to the absence of absorption reactions they have a long mean free path and leave the matter undistorted by strong final state interactions. Moreover, at subthreshold energies nucleons have to accumulate energy by multiple

scattering processes in order to overcome the threshold for kaon production and therefore these processes should be particularly sensitive to collective effects. Within the last decade the KaoS Collaboration has performed systematic measurements of the K^+ production far below threshold, see Refs. 55, 56, 57, 58, 59. Based on the new data situation, in Ref. 60 the question if valuable information on the nuclear EOS can be extracted has been revisited and it has been shown that subthreshold K^+ production provides indeed a suitable and reliable tool for this purpose. These results have been confirmed by the Nantes group later on 61. In subsequent investigations the stability of the EOS dependence has been proven, Refs. 62, 21, 63. Excitation functions from KaoS 59, 57 are shown in Fig. 8 and compared to

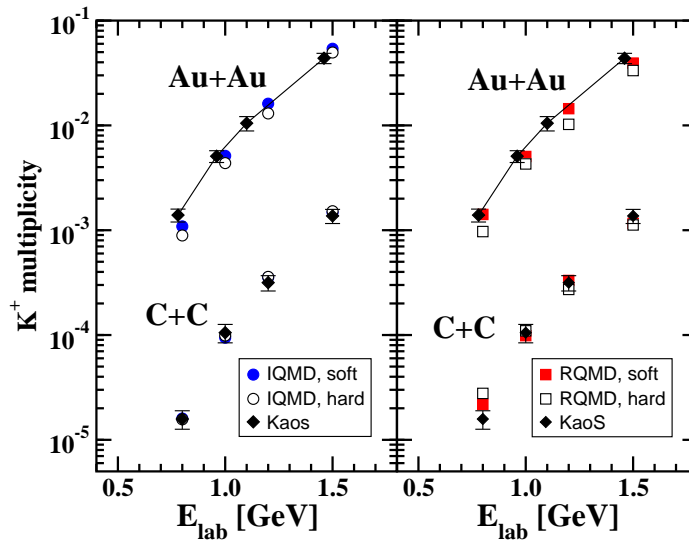


Fig. 8. Excitation function of the K^+ multiplicities in $Au + Au$ and $C + C$ reactions. RQMD 60 and IQMD 63 with in-medium kaon potential and using a hard/soft nuclear EOS are compared to data from the KaoS Collaboration 59.

RQMD 60, 21 and IQMD 63 calculations. As expected the EOS dependence is pronounced in the $Au + Au$ system while the light $C + C$ system serves as a calibration. The effects become even more evident when the ratio R of the kaon multiplicities obtained in $Au + Au$ over $C + C$ reactions (normalised to the corresponding mass numbers) is built 60, 59. Such a ratio has the advantage that possible uncertainties which might still exist in the theoretical calculations should cancel out to large extent. This ratio is shown

in Fig. 9. Both, soft and hard EOS, show an increase of R with decreasing energy down to 1.0 AGeV. However, this increase is much less pronounced when the stiff EOS is employed. The comparison to the experimental data from KaoS⁵⁹, where the increase of R is even more pronounced, strongly favours a soft equation of state. Fig. 9 demonstrates also the robustness

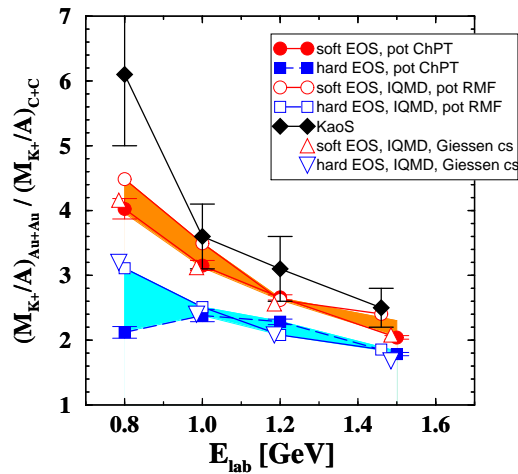


Fig. 9. Excitation function of the ratio R of K^+ multiplicities obtained in inclusive Au+Au over C+C reactions. RQMD⁶⁰ and IQMD⁶³ calculations are compared to KaoS data⁵⁹. Figure is taken from²¹.

of this observable. Exploring the range of uncertainty in the corresponding transport calculations the stability of the conclusions drawn from this observable has been demonstrated in Ref.⁶³. This concerns elementary input, in particular the elementary production cross sections $N\Delta; \Delta\Delta \mapsto NYK^+$ which are not constrained by data.

2.3. Constraints from neutron stars

Measurements of “extreme” values, like large masses or radii, huge luminosities etc. as provided by compact stars offer good opportunities to gain deeper insight into the physics of matter under extreme conditions. There has been substantial progress in recent time from the astrophysical side.

The most spectacular observation was probably the recent measurement⁶⁴ on PSR J0751+1807, a millisecond pulsar in a binary system

with a helium white dwarf secondary, which implies a pulsar mass of $2.1 \pm 0.2 \left(\begin{smallmatrix} +0.4 \\ -0.5 \end{smallmatrix} \right) M_{\odot}$ with 1σ (2σ) confidence. Therefore, a reliable EOS has to describe neutron star (NS) masses of at least $1.9 M_{\odot}$ (1σ) in a strong, or $1.6 M_{\odot}$ (2σ) in a weak interpretation. This condition limits the softness of EOS in NS matter. One might therefore be worried about an apparent contradiction between the constraints derived from neutron stars and those from heavy ion reactions. While heavy ion reactions favor a soft EOS, PSR J0751+1807 requires a stiff EOS. The corresponding constraints are, however, complementary rather than contradictory. Intermediate energy heavy-ion reactions, e.g. subthreshold kaon production, constrains the EOS at densities up to $2 \div 3 \rho_0$ while the maximum NS mass is more sensitive to the high density behaviour of the EOS. Combining the two constraints implies that the EOS should be *soft at moderate densities and stiff at high densities*. Such a behaviour is predicted by microscopic many-body calculations (see Fig. 2). DBHF, BHF or variational calculations, typically, lead to maximum NS masses between $2.1 \div 2.3 M_{\odot}$ and are therefore in accordance with PSR J0751+1807, see Ref. ⁶⁵.

There exist several other constraints on the nuclear EOS which can be derived from observations of compact stars, see e.g. Refs. ^{65, 66, 67}. Among these, the most promising one is the Direct Urca (DU) process which is essentially driven by the proton fraction inside the NS ⁶⁸. DU processes, e.g. the neutron β -decay $n \rightarrow p + e^{-} + \bar{\nu}_e$, are very efficient regarding their neutrino production, even in superfluid NM ^{69, 70}, and cool NSs too fast to be in accordance with data from thermally observable NSs. Therefore, one can suppose that no DU processes should occur below the upper mass limit for “typical” NSs, i.e. $M_{DU} \geq 1.5 M_{\odot}$ ($1.35 M_{\odot}$ in a weak interpretation). These limits come from a population synthesis of young, nearby NSs ⁷¹ and masses of NS binaries ⁶⁴.

3. Summary

The status of theoretical models which make predictions for the EOS can roughly be summarized as follows: phenomenological density functionals such as Skyrme, Gogny or relativistic mean field models provide high precision fits to the nuclear chart but extrapolations to supra-normal densities or the limits of stability are highly uncertain. A more controlled way provide effective field theory approaches which became quite popular in recent time. Effective chiral field theory allows e.g. a systematic generation of two- and many-body nuclear forces. However, these approaches are low momentum expansions and when applied to the nuclear many-body problem, low den-

sity expansions. Ab initio calculations for the nuclear many-body problem such as variational or Brueckner calculations have reached a high degree of sophistication and can serve as guidelines for the extrapolation to the regimes of high density and/or large isospin asymmetry. Possible future developments are to base such calculations on modern EFT potentials and to achieve a more consistent treatment of two- and three-body forces.

If one intends to constrain these models by nuclear reactions one has to account for the reaction dynamics by semi-classical transport models of a Boltzmann or molecular dynamics type. Suitable observables which have been found to be sensitive on the nuclear EOS are directed and elliptic collective flow pattern and particle production, in particular kaon production, at higher energies. Heavy ion data suggest that the EOS of symmetric nuclear matter shows a soft behavior in the density regime between one to about three times nuclear saturation density, which is consistent with the predictions from many-body calculations. Conclusions on the EOS are, however, complicated by the interplay between the density and the momentum dependence of the nuclear mean field. Data which constrain the isospin dependence of the mean field are still scarce. Promising observables are isospin diffusion, iso-scaling of intermediate mass fragments and particle ratios (π^+/π^- and eventually K^+/K^0 ⁷²). Here the situation will certainly improve when the forthcoming radioactive beam facilities will be operating.

References

1. GSI Conceptual Design Report, <http://www.gsi.de/GSI-Future>
2. RIA homepage, <http://www.orau.org/ria>
3. C. Fuchs, H.H. Wolter, [nucl-th/0511070] Euro. Phys. J. A in press.
4. M. Kleban, B. Nerlo-Pomorska, J. F. Berger, J. Decharge, M. Girod, S. Hilaire, Phys. Rev. C **65**, 024309 (2002).
5. B. Cochet, K. Bennaceur, J. Meyer, P. Bonche, T. Duguet, Int. J. Mod. Phys. **E13**, 187 (2004).
6. P.-G. Reinhard, M. Bender, Lect. Notes Phys. **641**, 249 (2004).
7. P. Ring, Prog. Part. Nucl. Phys. **73**, 193 (1996); Lect. Notes Phys. **641**, 175 (2004).
8. B.D. Serot, J.D. Walecka, Int. J. Mod. Phys. **E6**, 515 (1997).
9. R.J. Furnstahl, Lect. Notes Phys. **641**, 1 (2004).
10. M. Lutz, B. Friman, Ch. Appel, Phys. Lett. **B474**, 7 (2000).
11. P. Finelli, N. Kaiser, D. Vretenar, W. Weise, Eur. Phys. J. **A17**, 573 (2003); Nucl. Phys. **A735**, 449 (2004).
12. D. Vretenar, W. Weise, Lect. Notes Phys. **641**, 65 (2004).
13. A. Akmal, V.R. Pandharipande, D.G. Ravenhall, Phys. Rev. C **58**, 1804 (1998).

14. W. Zuo, A. Lejeune, U. Lombardo, J.F. Mathiot, Nucl. Phys. **A706**, 418 (2002).
15. X.R. Zhou, G.F. Burgio, U. Lombardo, H.-J. Schulze, W. Zuo, Phys. Rev. C **69**, 018801 (2004).
16. B. ter Haar, R. Malfliet, Phys. Rep. **149**, 207 (1987).
17. T. Gross-Boelting, C. Fuchs, A. Faessler, Nucl. Phys. **A648**, 105 (1999).
18. E. van Dalen, C. Fuchs, A. Faessler, Nucl. Phys. **A744**, 227 (2004); Phys. Rev. C **72**, 065803 (2005).
19. W.H. Dickhoff, C. Barbieri, Prog. Part. Nucl. Phys. **52**, 377 (2004).
20. J. Carlson, J. Morales, V.R. Pandharipande, D.G. Ravenhall, Phys. Rev. C **68**, 025802 (2003).
21. C. Fuchs, Prog. Part. Nucl. Phys. **56**, 1 (2006).
22. K.A. Brueckner, J.L. Gammel, Phys. Rev. **107**, 1023 (1958)
23. R. Machleidt, K. Holinde, Ch. Elster, Phys. Rep. **149**, 1 (1987)
24. R. Brockmann, R. Machleidt, Phys. Rev. C **42**, 1965 (1990).
25. C. Fuchs, Lect. Notes Phys. **641**, 119 (2004).
26. D.R. Entem, R. Machleidt, Phys. Rev. C **68**, 041001 (2003).
27. E. Epelbaum, W. Glöckle, U.-G. Meissner, Nucl. Phys. **A747**, 362 (2005).
28. S.K. Bogner, T.T.S. Kuo, A. Schwenk, Phys. Rep. **386**, 1 (2003).
29. S.K. Bogner, A. Schwenk, R.J. Furnstahl, A. Nogga, Nucl. Phys. **A763**, 59 (2005).
30. G.A. Lalazissis, J. König, P. Ring, Phys. Rev. C **55**, 540 (1997).
31. S. Typel, H.H. Wolter, Nucl. Phys. **A656**, 331 (1999).
32. V. Baran, M. Colonna, V. Greco, M. Di Toro, Phys. Rep. **410**, 335 (2005).
33. T. Nikšić, D. Vretenar, P. Ring, Phys. Rev. C **66**, 064302 (2002).
34. C. Mahaux, P.F. Bortignon, R.A. Broglia, C.H. Dasso, Phys. Rep. **120**, 1 (1985).
35. D. Lunney, J.M. Pearson, C. Thibault, Rev. Mod. Phys. **75**, 1021 (2003).
36. E. van Dalen, C. Fuchs, A. Faessler, Phys. Rev. Lett. **95**, 022302 (2005).
37. M. Jaminon, C. Mahaux, Phys. Rev. C **40**, 354 (1989).
38. T. Frick, Kh. Gad, H. Müther, P. Czerski, Phys. Rev. C **65**, 034321 (2002).
39. J.M. Pearson, S. Goriely, Phys. Rev. C **64**, 027301 (2001).
40. F. de Jong, H. Lenske, Phys. Rev. C **58**, 890 (1998).
41. S. Hama *et al.*, Phys. Rev. C **41**, 2737 (1990); E.D. Cooper *et al.*, Phys. Rev. C **47**, 297 (1993).
42. P. Danielewicz, Nucl. Phys. **A673**, 275 (2000).
43. T. Gaitanos, C. Fuchs, H.H. Wolter, A. Faessler, Eur. Phys. J. **A12**, 421 (2001).
44. P.K. Sahu, W. Cassing, U. Mosel, A. Ohnishi, Nucl. Phys. **A672**, 376 (2000).
45. H.F. Arellano, H.V. von Geramb, Phys. Rev. C **66**, 024602 (2002).
46. S. Typel, Phys. Rev. C **71**, 064301 (2005).
47. W. Zuo, L.G. Cao, B.A. Li, U. Lombardo, C.W. Shen, Phys. Rev. C **72**, 014005 (2005).
48. T. Gaitanos, M. Di Toro, S. Typel, V. Baran, C. Fuchs, V. Greco, H.H. Wolter Nucl. Phys. **A732**, 24 (2004).
49. L.-W. Chen, C.M. Ko, B.-A. Li, Phys. Rev. C **72**, 064606 (2005).

50. J.A. McNeil, J.R. Shepard, S.J. Wallace, *Phys. Rev. C* **27**, 2123 (1983).
51. A.M. Lane, *Nucl. Phys.* **35**, 676 (1962).
52. R. Kozack, D.G. Madland, *Phys. Rev. C* **39**, 1461 (1989); *Nucl. Phys.* **A509**, 664 (1990).
53. R. Stock, *Phys. Rep.* **135**, 259 (1986).
54. J. Aichelin and C.M. Ko, *Phys. Rev. Lett.* **55**, 2661 (1985).
55. D. Miskowiec et al. [KaoS Collaboration], *Phys. Rev. Lett.* **72**, 3650 (1994).
56. R. Barth et al. [KaoS Collaboration], *Phys. Rev. Lett.* **78**, 4007 (1997).
57. F. Laue et al. [KaoS Collaboration], *Phys. Rev. Lett.* **82**, 1640 (1999).
58. F. Laue et al. [KaoS Collaboration], *Eur. Phys. J.* **A9**, 397 (2000).
59. C. Sturm et al. [KaoS Collaboration], *Phys. Rev. Lett.* **86**, 39 (2001).
60. C. Fuchs, Amand Faessler, E. Zabrodin, Y.M. Zheng, *Phys. Rev. Lett.* **86**, 1974 (2001).
61. Ch. Hartnack, J. Aichelin, *J. Phys. G* **28**, 1649 (2002).
62. C. Fuchs, A. Faessler, S. El-Basaouny, E. Zabrodin, *J. Phys. G* **28**, 1615 (2002).
63. Ch. Hartnack, H. Oeschler, J. Aichelin, *Phys. Rev. Lett.* **96**, 012302 (2006).
64. D.J. Nice, E.M. Splaver, I.H. Stairs, O. Löhmer, A. Jessner, M. Kramer, and J.M. Cordes, *Astrophys. J.* **634**, 1242 (2005).
65. T. Kähn et al., *Phys. Rev. C* **74**, 035802 (2006).
66. A.W. Steiner, M. Prakash, J.M. Lattimer, P.J. Ellis, *Phys. Rep.* **411**, 325 (2005).
67. B.-A. Li, A.W. Steiner, [nucl-th/0511064].
68. J.M. Lattimer, C.J. Pethick, M. Prakash, and P. Haensel, *Phys. Rev. Lett.* **66**, 2701 (1991).
69. D. Blaschke, H. Grigorian, and D. Voskresensky, *Astron. Astrophys.* **424**, 979 (2004).
70. E.E. Kolomeitsev, and D.N. Voskresensky, *Nucl.Phys. A* **759**, 373 (2005).
71. S. Popov, H. Grigorian, R. Turolla and D. Blaschke, *Astron. Astrophys.* **448**, 327 (2006).
72. G. Ferini, T. Gaitanos, M. Colonna, M. Di Toro, H.H. Wolter, [nucl-th/0607005].